Measurement-Based Real-Time Security-Constrained Economic Dispatch

Kai E. Van Horn *Student Member*, *IEEE*, Alejandro D. Domínguez-García *Member*, *IEEE*, and Peter W. Sauer *Life Fellow*, *IEEE*

***Abstract*—In this paper, we propose a measurement-based approach to the real-time security-constrained economic dispatch (SCED). The real-time SCED is a widely used market scheduling tool that seeks to economically balance electricity system supply and demand and provide locational marginal prices (LMPs) while ensuring system reliability standards are met. To capture network flows and security considerations, the conventional SCED relies on sensitivities that are typically computed from a linearized power flow model, which is vulnerable to phenomena such as undetected topology changes, changes in the system operating point, and the existence of incorrect model data. Our approach to the formulation of the SCED problem utilizes power system sensitivities estimated from phasor measurement unit (PMU) measurements. The resulting measurement-based real-time SCED is robust against the aforementioned phenomena. Moreover, the dispatch instructions and LMPs calculated with the proposed measurement-based SCED accurately reflect real-time system conditions and security needs. We illustrate the strengths of the proposed approach via several case studies.**

***Index Terms*—Economic Dispatch, Contingency Analysis, Estimation, Security, Distribution Factors, Operations, PMU.**

I. Introduction

The majority of electricity consumers in the United States are served by entities that procure energy in Independent System Operator (ISO)- or Regional Transmission Organization (RTO)-run markets [1]. ISO/RTOs oversee scheduling procedures consisting of a sequence of forward markets based on security-constrained unit commitment- and economic dispatch-based algorithms (see, e.g., [2], [3]). The goal of these processes is to schedule resources on various time-scales such that the system operator can maintain the supply-demand balance around-the-clock, and satisfy operational and physical constraints imposed by the electricity network and reliability standards. Moreover, the market outcomes include resource dispatch targets and the prices for energy, the locational marginal prices (LMPs), and ancillary services [4], which provide important economic signals to participants. The so-called real-time markets are the final stage in the market scheduling process, and real-time security-constrained economic dispatch (SCED), which relies on accurate contingency selection and analysis, is a key component of that stage. Typically, the real-time SCED is formulated using model-based linear flow sensitivities, known as injection shift factors (ISFs), to represent network flows [5]. In this work, we propose a measurement-based approach to the real-time SCED.

The authors are with the Department of Electrical and Computer Engineering of the University of Illinois at Urbana-Champaign, Urbana, IL, 61801, USA. E-mail: {kvanhor2, aledan, psauer}@illinois.edu.

In the power system real-time operational context, system operators are primarily concerned with economically maintaining *system security*. The system is said to be in a secure state when resource dispatch targets and other controllable system resources are set such that the supply-demand balance is met and so that the system can tolerate the failure of a small number of components without jeopardizing continued operation [6]. To achieve secure operation, system operators have conventionally undertaken three security functions: (i) system monitoring, (ii) contingency analysis, and (iii) security-constrained optimal power flow (SCOPF) [5]. System monitoring consists of collecting and processing measurements, e.g., voltages, power injections, or breaker statuses, for use in real-time applications. Contingency analysis harnesses the data from system monitoring along with a system model to perform model-based dc and ac power flow analyses to identify outages in the system that may cause overloads on system equipment and thus compromise system security. The overloads identified by contingency analysis are utilized with system operational constraints and system model data to formulate the real-time SCED—the formulation of the SCOPF used in real-time operations.

The SCED was first formulated more than 40 years ago [7]. Over the years, SCED research has focused on improving computational speed and incorporating additional system and reliability information, e.g., transient stability constraints and remedial actions, into the SCED problem formulation (see, e.g., [8]). More recent developments in methods for improving SCED solution computation times have focused on reducing the size of the problem, e.g., by eliminating unnecessary constraints (see e.g., [9]), or by decomposing the problem into a series of less computationally burdensome subproblems via methods such as Benders' decomposition (see, e.g., [10]). Furthermore, the introduction of market-based scheduling for electricity and reserves necessitates more complex formulations of the SCED (see, e.g., [11]). Also, in the past two decades, improvements in optimization methods and the availability and economy of computational resources have driven a surge in the exploration of probabilistic methods for incorporating reliability considerations into the SCED (see, e.g., [12]). In this paper, we focus on a deterministic single-stage linear formulation of the SCED, which, to our knowledge, is the formulation commonly used in practice (see, e.g. [2], [3]).

In order to perform conventional contingency analysis and formulate power flow, network flow, and security constraints in the real-time SCED, the system operator requires an up-to-date

model of the ISO/RTO's electricity system and that of neighboring systems, which is typically derived from the output of a state estimator. The state estimator-based model is vulnerable to errors due to numerous phenomena, e.g., undetected changes in the internal system topology and erroneous model parameters [13], as well as inaccurate representations of neighboring systems [14]. Further, model line parameters errors can arise as a result of assumptions made when computing model parameter values, e.g., the extent of line transposition and non-homogeneity in conductor material due to partial facility upgrades/reconductoring [15]. Also, model parameter values are impacted dynamically by natural phenomena, e.g., mutual conductance, temperature, humidity, and ground conductance [16]. The accuracy of security constraints identified through contingency analysis and the dispatch targets and LMPs determined in the model-based real-time SCED are coupled with the accuracy of the system model and, as such, subject to the same vulnerabilities. Inaccurate contingency analysis, dispatch targets, and LMPs have economic implications, e.g., sending incorrect local price signals and over/under payment to resources, as well as system reliability implications, e.g., unintended equipment overloads and outages [17], [18], [19].

In this paper, we propose a measurement-based approach to the real-time SCED with the goal of overcoming the shortcomings of the model-based SCED described above. The crux of our approach is the reformulation of the SCED constraints using more accurate data—removing model-based quantities and replacing them with measurement-based estimates of the same quantities. Specifically, we reformulate two types of constraints: (i) network flow constraints, and (ii) security constraints. In the model-based SCED, both of these types of constraints depend on model-based ISFs and sensitivities derived from ISFs. Instead of relying on model-based ISFs, our approach utilizes the measurement-based method for estimating sensitivities described in [20] and [21].

By moving away from a model-based representation of the network, our approach virtually eliminates the impacts of phenomena such as undetected changes in system topology and erroneous model parameters on the real-time SCED outcomes. Furthermore, by computing sensitivities directly from measurements, the measurement-based SCED can be formulated without the output of a topology processor and state estimator, which may be advantageous for cases in which the state estimator fails to converge (see, e.g., [17], [18]). Our measurement-based approach also removes the requirement to define an arbitrary distributed slack bus policy in order to compute the ISFs, which is a fundamental limitation of model-based ISFs. Finally, the measurement-based sensitivities can be used to enhance contingency selection, which, as we show, can improved contingency analysis by identifying potential cases of security constraint omission and commission due to model errors that will subsequently impact the SCED formulation and solution.

Our approach relies on the availability of phasor measurement units (PMUs), the preponderance of which in power systems is facilitating the proliferation of a new generation of operational tools that harness the very high frequency and time synchronicity of their measurements (see, e.g., [22], [23]). The use of PMU data in real-time operations has been promoted as a means by which to circumvent the shortcomings of the existing telemetry system, and reduce the frequency of occurrence and the magnitude of the impact of preventable outages [19]. As we show, the real-time contingency selection and SCED processes can likewise be enhanced by the deployment of PMU measurements.

Several approaches to identifying and handling erroneous data in state estimation have been proposed [24]. Further, ISOs/RTOs update system model data periodically as erroneous data are identified through ex-post analysis, e.g., the analysis of non-convergent state-estimator solutions, and reporting by market participants (see, e.g., [25]). However, even with these error detection and correction algorithms and processes in place, the potential for erroneous model data and topological errors persists in real-time operations and presents a challenge to reliable and economic power system operations. As discussed above, our proposed measurement-based SCED approach addresses this challenge by bypassing the need for a system model.

This paper extends in a number of directions the preliminary work reported in [26]. First, we give a detailed account of the advantages of applying measurement-based security assessment in real-time operations. Second, we formulate the *security-constrained* economic dispatch, whereas in [26] we did not consider system security. Finally, we furnish the results of case studies carried out on a larger test system to demonstrate the scalability of our approach.

The remainder of this paper is organized as follows. In Section II, we give an overview of conventional model-based contingency analysis and SCED. In Section III, we describe the measurement-based sensitivity estimation approach that we leverage in this work, as well as the application of measurement-based sensitivities in the context of the real-time contingency analysis and SCED. In Sections IV and V, we present the results of case studies carried out to demonstrate the strengths of the proposed measurement-based SCED. The final section reiterates the contributions of this work and points to some directions for future work.

II. Conventional Real-Time SCED

The SCED is a widely-used, optimal power flow (OPF)-based market scheduling tool that has four primary components: (i) power flow and network flow constraints obtained from a model of the system; (ii) equipment constraints, e.g., generator power output limits; (iii) reliability-driven constraints, e.g., reserve requirement and security constraints; and (iv) the objective, typically the maximization of social surplus or minimization of generator costs, commonly quadratic or piecewise-linear functions (see, e.g., [5], [7], [27]).

For a number of computational and practical reasons, the conventional real-time SCED is commonly formulated using a simplified OPF formulation, referred to as the DC-OPF [28]. The DC-OPF relies on the so-called "dc" assumptions: (i) the system is lossless, (ii) the voltage at each bus is approximately equal to one p.u., (iii) the difference in the voltage angles between each pair of connected buses is small [5]. These

assumptions result in a linear approximation of the nonlinear power flow and network flow constraints.

A. Power Balance

To formulate the real-time SCED, we consider a system that consists of N buses indexed by $\mathcal{N} = \{1, \ldots, N\}$, and L lines indexed by $\mathcal{L} = \{\ell_1, \ldots, \ell_L\}$, where each ℓ_l is an ordered pair (n, m), $n, m \in \mathcal{N}$, representing a transmission line between buses n and m, with the convention that positive flow on such a line is in the direction *from* n *to* m. Moreover, let there be G generators indexed by $\mathcal{G} = \{1, \ldots, G\}$, and D loads indexed by $\mathcal{D} = \{1, \ldots, D\}$. Let $\mathcal{G}_n \subseteq \mathcal{G}$ be the subset of generators at bus $n \in \mathcal{N}$, and let $\mathcal{D}_m \subseteq \mathcal{D}$ be the subset of loads at bus $m \in \mathcal{N}$.

Let P_i^g be the output of generator $i \in \mathcal{G}$, with the convention that $P_i^g > 0$ if generator i injects real power into the system; and let P_v^d be the demand of load $v \in \mathcal{D}$, with the convention that $P_v^d > 0$ if load j withdraws real power from the system. Then, define the vectors of generation and demand as $P^g = [P_1^g, \ldots, P_G^g]^T$ and $P^d = \left[P_1^d, \ldots, P_D^d\right]^T$, respectively. With these quantities, we define the net injection at a bus $n \in \mathcal{N}$ as

$$P_n = \sum_{i \in \mathcal{G}_n} P_i^g - \sum_{v \in \mathcal{D}_n} P_v^d, \tag{1}$$

with the convention that $P_n > 0$ if real power is injected *into* the system. Then, define the vector of net injections at all buses as $P = [P_1, \ldots, P_N]^T$.

In the ISF-based network representation, the voltage angles are not explicitly represented, rather the bus power balance and power flowing on each line are written in terms of the system-wide power balance, the linear flow sensitivities, and the bus injections. The system-wide power balance constraint is given by

$$\mathbb{1}_G^T P^g - \mathbb{1}_D^T P^d - P^\ell = 0, \tag{2}$$

where $\mathbb{1}_G$ and $\mathbb{1}_D$ are all-ones vectors of dimensions G and D, respectively; and P^ℓ is system-wide losses, which we will assume takes the form of a sensitivity-factor-based loss model, such as that given in [29].

B. Network Flow Constraints

Let $A = [a_1, \ldots, a_i, \ldots, a_N]$ denote the transmission network incidence matrix, where a_i is an L-dimensional column vector the jth entry of which is equal to 1 if bus i is the *from* bus of line j, -1 if bus i is the *to* bus of line j, and zero otherwise. Further, let b denote the L-dimensional column vector of branch susceptances, and define the diagonal $L \times L$ branch susceptance matrix as $B_b = \text{diag}\{b\}$, where $\text{diag}\{\cdot\}$ denotes a diagonal matrix such that $B_b[i, i] = b_i$, $\forall i$. Then, define the $(N-1)\times(N-1)$ reduced nodal susceptance matrix as $B = \tilde{A}^T B_b \tilde{A}$, where $\tilde{A}$ is the incidence matrix absent the column corresponding to the specified slack bus.

The $L \times N$ linear flow sensitivity matrix, or ISF matrix, denoted by Ψ, provides the basis of the ISF-based DC-OPF network flow representation. An entry of Ψ, denoted by $\Psi[l, i]$, provides the sensitivity of the flow on line $\ell_l \in \mathcal{L}$ to an injection at bus i that is withdrawn at the slack bus. Under the DC assumptions, Ψ can be calculated directly from the network connectivity and parameters as follows [5]

$$\Psi = B_b A B^{-1}, \tag{3}$$

where we assume that Ψ has been augmented in the appropriate location with a column of zeros corresponding to the slack bus such that it is of dimensions $L \times N$.

With the model-based ISFs from (3), we define the vector of line flows in terms of the bus injections as

$$P^f = \Psi P, \tag{4}$$

which are bounded above and below by the line upper and lower limits, denoted by $\bar{P}^f$ and $\underline{P}^f$, respectively.

C. Security Constraints

Power systems are typically operated with the so-called *"N-1" security* criterion, i.e., no equipment will be overloaded by the outage of a single line, generator, or other facility. To ensure that this requirement is upheld in the solution of the real-time SCED, *security constraints* are added to the formulation. These constraints incorporate the *post-contingency* behavior of the system into the real-time SCED so that the resulting dispatch is secure under such contingencies. In this work, we consider a deterministic formulation of the SCED with no corrective actions, i.e., no decision variables for post-contingency reconfiguration of system resources. Such a formulation is a *preventative* approach to ensuring system security, and is consistent with current practice in ISO/RTO-run markets [8]. Alternative SCED formulations, which include the possibility of post-contingency reconfiguration of system resources in response to contingencies (see, e.g., [10] ,[12], [30]), have been proposed, but, to our knowledge, their deployment has so far been limited in scope.

In order to select the contingencies for which security constraints will be formulated, the system operator undertakes contingency selection and analysis so as to ascertain the contingencies, e.g., line and generator outages, that will result in overloads on system equipment. In practice, operators do not consider the impacts of every possible single outage on every piece of equipment, e.g., line, transformer, in the system, rather they consider a subset of facilities and contingencies via a pre-defined set of so-called *mon-con pairs*—each mon-con pair specifies a monitored facility and the contingency with respect to which it is monitored for overloads.

To be useful in the real-time operational context, real-time contingency analysis must be executed in a timely fashion (on the order of minutes, see, e.g. [31]) . As such, contingency analysis is conducted using a contingency list composed of a subset of all possible mon-con pairs, which are selected using a combination of off-line studies, operator discretion, and dc-analysis, e.g., the flow performance index [5]. Ac power flow-based contingency analysis is used to analyze each mon-con pair on the contingency list, i.e., those contingencies deemed to have significant potential to degrade system security. The outcome of contingency analysis is a set of mon-con pairs for which the corresponding outages cause overloads and for which security constraints must be included in the SCED.

Power system sensitivities, namely the power transfer distribution factors (PTDFs) and line outage distribution factors (LODFs), are essential to the formulation of security constraints [5]. The $N \times N$ matrix of PTDFs for a line ℓ_l, denoted by Φ_l, provides the sensitivity of the flow on line ℓ_l to real-power transactions between buses in the system, e.g., the (n,m)th element of Φ_l, denoted by $\Phi_l[n,m]$, gives us the proportion of a real power transaction injected at bus n and withdrawn at bus m that flows over line ℓ_l. The PTDF for a line ℓ_l with respect to an injection at a bus n that is withdrawn at a bus m is calculated directly from the ISFs as follows [5]:

$$\Phi_l[n,m] = \Psi[l,n] - \Psi[l,m]. \tag{5}$$

The $L \times L$ matrix of LODFs provides the proportion of the pre-outage flow on each line ℓ_l that flows on each in-service line ℓ_u in the system in the event of the outage of line ℓ_l . The LODF for a line ℓ_u with respect to the outage of a separate line $\ell_l = (n,m)$ is calculated from the PTDFs in (5) of the respective lines by [5]

$$\Xi[u,l] := \frac{\Phi_u[n,m]}{1 - \Phi_l[n,m]}. \tag{6}$$

Let $\mathcal{C}^g$ and $\mathcal{C}^f$ be the sets of generator and line outage mon-con pairs, respectively, identified by the system operator through contingency analysis as causing overloads. The sets $\mathcal{C}^g$ and $\mathcal{C}^f$ consist of doubles of the form (ℓ_u, c_j^g) and (ℓ_u, c_l^f), respectively, where (ℓ_u, c_j^g) is the mon-con pair for the overload of monitored line ℓ_u with respect to the outage of generator j and (ℓ_u, c_l^f) is similarly defined for line outage mon-con pairs.

We formulate a security constraint for each line outage mon-con pair, $(\ell_u, c_l^f) \in \mathcal{C}^f$, using the LODFs from (6) as follows

$$\underline{P}_u^f \leq \Psi_u P + \Xi[u,l]\Psi_l P \leq \bar{P}_u^f, \tag{7}$$

where Ψ_u and Ψ_l are the uth and lth rows, respectively, of the ISF matrix. Then, define Ψ^f as the matrix of line flow to bus injection sensitivities for all line outages, where each row m corresponds to a mon-con pair $(\ell_u, c_l^f) \in \mathcal{C}^f$ and is given by

$$\Psi_m^f = \Psi_u + \Xi[u,l]\Psi_l. \tag{8}$$

The line flow impacts of generator contingencies depends on the response of the remaining generators in the system, which is typically approximated by a function of each generator's inertial constant, maximum capacity, or dispatchable range [5]. For the contingency of a generator j, we assume the generators remaining online respond according to pre-specified participation factors corresponding to the outage of generator j. Define the participation factor of each generator i corresponding to the outage of generator j by

$$\alpha_i^g(c_j^g) = \begin{cases} \frac{\bar{P}_i^g}{\sum_{i \in \mathcal{G}, i \neq j} \bar{P}_i^g} & \text{if } i \neq j, i \in \mathcal{G}, \\ -1 & \text{if } i = j, i \in \mathcal{G}, \\ 0 & \text{otherwise.} \end{cases} \tag{9}$$

Then, let $\alpha(c_j^g)$ be the N-dimensional vector of nodal generator participation factors corresponding to the outage of generator j, each entry of which is given by

$$\alpha_n(c_j^g) = \sum_{i \in \mathcal{G}_n} \alpha_i^g(c_j^g). \tag{10}$$

For notational convenience, and without loss of generality, we assume there are no loads at the generator buses. Using the participation factors from (10), we formulate a security constraint for each generator outage mon-con pair, $(\ell_u, c_j^g) \in \mathcal{C}^g$, as follows

$$\underline{P}_u^f \leq \Psi_u P + (\Psi_u \alpha(c_j^g) e_j^T) P \leq \bar{P}_u^f, \tag{11}$$

where e_j is an N-dimensional vector with a one in the jth entry and a zero in each other entry. Define Ψ^g as the matrix of line flow to bus injection sensitivities for the generator outages, where each row m corresponds to a mon-con pair $(\ell_u, c_j^g) \in \mathcal{C}^g$ and is given by

$$\Psi_m^g = \Psi_u + (\Psi_u \alpha(c_j^g)) e_j^T. \tag{12}$$

Furthermore, to ensure reliability is not compromised by a generator outage, there must be adequate upward capacity among all generators in the system to respond to the outage. Such limitations are typically captured by reserve constraints in the SCED. Though critically important for maintaining reliability, the reserve constraints are not directly impacted by the measurement-based formulation proposed here and so, for the sake of brevity, we do not explicitly represent them in the formulation.

Let $\underline{P}^s$, $\bar{P}^s$, be the vectors of lower and upper security constraint limits, respectively, which consist of the line limits corresponding to the potentially overloaded lines of their respective security constraints. Then, we can concisely state the collection of security constraints corresponding to those mon-con pairs in $\mathcal{C}^f$ and $\mathcal{C}^g$ and defined in (7) and (11), respectively, as

$$\underline{P}^s \leq \Psi^s P \leq \bar{P}^s, \tag{13}$$

where

$$\Psi^s = \begin{bmatrix} \Psi^f \\ \Psi^g \end{bmatrix}. \tag{14}$$

D. Model-Based Real-Time SCED Problem Formulation

Let $\mathscr{O}_i(\cdot)$ be the offer function of generator i and $\mathscr{B}_j^d(\cdot)$ be the bid function of demand j, the arguments of which are P_i^g and P_j^d, respectively. The objective of the real-time SCED is the maximization of the social surplus [27], which is defined as

$$\mathscr{S}(P^g, P^d) = \sum_{v \in \mathcal{D}} \mathscr{B}_v(P_v^d) - \sum_{i \in \mathcal{G}} \mathscr{O}_i(P_i^g). \tag{15}$$

Combining the objective in (15) with the constraints that result from the power balance and network flow expressions in (2) and (4), respectively, and the security constraints in (13) we

formulate the model-based real-time SCED as follows

$$\max_{P^g,P^d} \mathscr{S}(P^g,P^d) \tag{16a}$$

$$s.t.$$

$$\mathbb{1}_G P^g - \mathbb{1}_D P^d - P^\ell = 0 \leftrightarrow \lambda_r \tag{16b}$$

$$\underline{P}^g \le P^g \le \bar{P}^g \tag{16c}$$

$$\underline{P}^d \le P^d \le \bar{P}^d \tag{16d}$$

$$\underline{P}^f \le \Psi P \le \bar{P}^f \qquad \leftrightarrow \underline{\mu}^f, \bar{\mu}^f \tag{16e}$$

$$\underline{P}^s \le \Psi^s P \le \bar{P}^s \qquad \leftrightarrow \underline{\mu}^s, \bar{\mu}^s, \tag{16f}$$

where $\underline{P}^g(\bar{P}^g)$ and $\underline{P}^d(\bar{P}^d)$ are the vectors of generator and load lower (upper) limits, respectively, and λ_r, $\underline{\mu}^f, \bar{\mu}^f$, and $\underline{\mu}^s, \bar{\mu}^s$ are the dual variables of their respective constraints, also referred to as *shadow prices* due to their well-known economic interpretation [27]. The shadow price of the system-wide power balance constraint, λ_r, is often referred to as the system reference or energy price. Note that for clarity of presentation in (16), we have left out of the real-time SCED the reserve requirement and ramping constraints that are often present in a practical real-time SCED [4]. The exclusion of these constraints, however, has no bearing on the formulation of the measurement-based real-time SCED and they may easily be included in our approach.

The primary outcomes of the real-time SCED are: (i) the optimal generator and load dispatch instructions, which are a direct result of the solution to (16); and (ii) the LMPs, which are not a direct result of the solution to (16), but may be calculated from the ISFs, the loss sensitivity vector, and the shadow prices [32].

Let ζ be the N-dimensional column vector of the sensitivity of system-wide losses to nodal injections. Then, the LMPs are computed as follows [33]:

$$\lambda = \lambda_r \mathbb{1}_N + \begin{bmatrix} \Psi \\ \Psi^s \end{bmatrix}^T \left(\begin{bmatrix} \bar{\mu}^f \\ \bar{\mu}^s \end{bmatrix} - \begin{bmatrix} \underline{\mu}^f \\ \underline{\mu}^s \end{bmatrix} \right) + \zeta \lambda_r, \tag{17}$$

where $\mathbb{1}_N$ is an N-dimensional all-ones vector. Now, define

$$\lambda^c = \begin{bmatrix} \Psi \\ \Psi^s \end{bmatrix}^T \left(\begin{bmatrix} \bar{\mu}^f \\ \bar{\mu}^s \end{bmatrix} - \begin{bmatrix} \underline{\mu}^f \\ \underline{\mu}^s \end{bmatrix} \right) \text{ and } \lambda^\ell = \zeta \lambda_r, \tag{18}$$

to be the N-dimensional vectors representing the congestion and loss components of the LMPs. The LMP expression in (17) is the so-called three-part LMP (see, e.g., [32], [33]), which consists of: (i) λ_r, the *energy component*, which represents the cost, from those generators that provide it, to generate the next MW; (ii) λ^c, the *congestion components*, which capture the additional costs to deliver the next MW to each bus associated with transmission congestion-driven dispatch limitations; and (iii) λ^ℓ, the *loss components*, which account for the location-differentiated cost of losses associated with serving the next MW at each bus.

III. Measurement-Based Real-Time SCED

It is clear from (16) that the dispatch targets and LMPs calculated from the results of the model-based real-time SCED depend heavily on the model-based ISFs and how accurately these ISFs reflect the conditions in the system at the time the real-time SCED is formulated. However, due to potential inaccuracies in telemetry and state estimation that may propagate to the underlying system model, the model-based ISFs may not always reflect the real-time system conditions.We address this shortcoming of the model-based SCED via the deployment of the measurement-based ISF approach proposed in [20].

A. Measurement-Based ISFs

Consider the same power system defined in Section II. Suppose the net real power injected into the system at bus n at time t, $P_n(t)$, varies by a small amount $\Delta P_n(t)$ from time t to time $t+\Delta t$, where $\Delta t > 0$ and small. Further, let $\Delta P_{l,n}(t)$ be the change in real power flow on line ℓ_l due to ΔP_n. Define the measurement-based ISF for line ℓ_l with respect to an injection at bus n as

$$\Gamma[l,n] := \frac{\partial P_l^f}{\partial P_n} \approx \frac{\Delta P_{l,n}^f}{\Delta P_n}. \tag{19}$$

While $\Delta P_{l,n}^f(t)$ is not directly available through PMU measurements, we can, however, measure $\Delta P_l^f(t)$, the total change in flow on line ℓ_l due to bus injections at time t. We observe that the variation in the flow on line ℓ_l is due to variations in the injections at each bus n:

$$\Delta P_l^f = \Delta P_{l,1}^f(t) + \cdots + \Delta P_{l,N}^f(t). \tag{20}$$

Employing (19) in (20) we obtain

$$\Delta P_l^f \approx \Delta P_1(t)\Gamma[l,1] + \cdots + \Delta P_N(t)\Gamma[l,N].$$

Now suppose we have $M+1$ sets of synchronized measurements. Let

$$\Delta P_n[k] = P_n[(k+1)\Delta t] - P_n[k\Delta t], \tag{21}$$

$$\Delta P_l^f[k] = P_l^f[(k+1)\Delta t] - P_l^f[k\Delta t], \tag{22}$$

for $j = 1,\ldots,M$ and define

$$\Delta P_n = [\Delta P_n[1] \ \cdots \ \Delta P_n[k] \ \cdots \ \Delta P_n[M]]^T, \tag{23}$$

$$\Delta P_l^f = \left[\Delta P_l^f[1] \ \cdots \ \Delta P_l^f[k] \ \cdots \ \Delta P_l^f[M]\right]^T. \tag{24}$$

Let $\Gamma_l = [\Gamma[l,1],\ldots,\Gamma[l,n],\ldots,\Gamma[l,N]]$. Then, clearly,

$$\Delta P_l^f = [\Delta P_1 \ \cdots \ \Delta P_n \ \cdots \ \Delta P_N]\,\Gamma_l^T. \tag{25}$$

Let ΔP denote the $M \times N$ matrix $[\Delta P_1 \ \cdots \ \Delta P_n \ \cdots \ \Delta P_N]$. Then, the system in (25) becomes

$$\Delta P_l^f = \Delta P \Gamma_l^T. \tag{26}$$

If $M \ge N$, then (26) is an overdetermined system. Moreover, assuming the ISFs are approximately constant over the $M+1$ measurements, we can obtain an estimate of Γ_l from least-squares error estimation as

$$\hat{\Gamma}_l^T = (\Delta P^T \Delta P)^{-1} \Delta P^T \Delta P_l^f. \tag{27}$$

1) Practical Considerations for the ISF Estimation: The estimation of the measurement-based ISF in (27) requires a complete set of data, i.e., M sets of injection and line flow measurements, where $M > N$. Moreover, it gives

equal weight to all measurements, regardless of when they were taken. In practice, these aspects of the approach above may prove to be impractical. To address this, [20] deploys a weighted least squares (WLS) formulation of (27) given by

$$\hat{\Gamma}_l^T = (\Delta P^T W \Delta P)^{-1} \Delta P^T W \Delta P_l^f, \tag{28}$$

where W is the weighting matrix, which can be selected to give more weight to recent measurements. Such an approach is advantageous for tracking changing operating conditions and minimizing the impacts of erroneous measurements. The WLS approach in (28) is further improved in [20] by the application of recursive weighted least squares, which enables the generation of updated estimates of the $\hat{\Gamma}_l$ as each set of measurements arrives, as opposed to the requirement in (27) of a complete set of measurements in order to perform the estimation. An alternative approach proposed in [21], applicable if $M < N$, is to estimate $\hat{\Gamma}_l$ using sparse vector recovery methods from Compressed Sensing. In this work, we adopt the WLS approach in (28) with a diagonal weighting matrix W, where $W[k,k] = f^{M-k}$ and $f \in (0,1]$, for the purpose of demonstrating the benefits of our measurement-based SCED formulation.

2) PMU Measurement Error Impacts: PMU measurement data may contain errors due to a host of issues, e.g., communication channel failure, inadequate maintenance and calibration of PMUs, and detection of such errors is an area of ongoing research [34]. The accuracy of measurement data used in conventional applications, e.g., state estimation, is commonly assessed via error residuals (see, e.g., [24]). Additionally, some erroneous data can be detected by analyzing: (i) measurement magnitude, e.g., are the measurements orders of magnitude too small or large to be plausible; and (ii) measurement consistency, e.g., do the measurements result in gross violations of Kirchhoff's laws. In this paper, we assume that standard checks have been performed on the PMU measurements prior to their use in sensitivity estimation. Furthermore, the impacts of temporary errors in measured data are minimized through the use of weighted least squares with a sliding measurement window and by setting $f < 1$. In the following section, we discuss the application of the measurement-based ISFs in the context of the real-time SCED.

B. Measurement-Based Network and Security Constraints

Our primary goal in this work is to leverage the measurement-based ISF estimation approach described above to remove the dependence on a system model of the SCED in (16). To this end, we reformulate the network and security constraints, (16e) and (16f), respectively.

1) Network Constraints: Let $\hat{\Gamma}$ be the $L \times N$ matrix of the measurement-based ISF estimates, each row of which is obtained from (28). As described in Section II, model-based ISFs form the basis of the network description in the real-time SCED. To remove the model dependence of (16), we deploy $\hat{\Gamma}$ to re-formulate the network constraints (16e) as

$$\underline{P}^f \leq \hat{\Gamma} P \leq \bar{P}^f. \tag{29}$$

With these reformulated network constraints, the real-time SCED constraints will be based on pre-contingency line flows that accurately reflect real-time conditions. The measurement-based ISFs are also instrumental to measurement-based contingency analysis and the formulation of security constraints.

2) Sensitivity-Based Contingency Selection: The measurement-based ISFs can also be used to compute the LODFs and PTDFs, which may subsequently be used to perform contingency selection and formulate security constraints. The application of the measurement-based ISFs in this context offers several substantial enhancement to the SCED. The adaptive nature of the measurement-based ISFs reduces or eliminates the impacts of model accuracies, e.g., erroneous model data or undetected changes in system topology, on: (i) the identification of contingencies and their relative severity during contingency selection; (ii) the identification, through contingency analysis, of those facilities in the system that will be overloaded by a given outage (by providing an accurate contingency list); and (iii) the formulation of security constraints that accurately reflect the impacts of outages and injections.

To conduct online measurement-based contingency selection, the system operator could deploy the measurement-based ISFs and LODFs to compute the impacts of all potential contingencies (or a pre-determined subset of all potential contingencies composed of a set larger than the current contingency list). For each potential outage of a line ℓ_l, the operator analyzes the flow impacts on each non-outage line ℓ_u as follows:

$$|\hat{\Gamma}_u P + \hat{\Xi}[u,l]\hat{\Gamma}_l P| \leq \bar{P}_u^f, \tag{30}$$

where $\hat{\Xi}[u,l]$ is the measurement-based estimate of the LODF of line ℓ_u with respect to the outage of line ℓ_l. Similarly, for each potential outage of a generator j, the operator analyzes the flow impacts on each line ℓ_u as follows:

$$|\hat{\Gamma}_u P + (\hat{\Gamma}_u \alpha(c_j^g) e_j^T) P| \leq \bar{P}_u^f. \tag{31}$$

If a generator or line contingency is found to cause an overload via (30) or (31), respectively, a mon-con pair for the contingency and each corresponding overloaded element is added to the contingency list, which is subsequently used in ac contingency analysis to populate $\mathcal{C}^f$ and $\mathcal{C}^g$.

Additionally, if the post-contingency flows computed with (30) or (31) conflict substantially with those computed using ac contingency analysis, e.g., if a flow difference of more than 40% is identified (greater than the flow error between the various ac and dc models studied in [28]), the system operator could flag a potential error in the ac system model, which could be investigate using methods such as "Parity Checking", which is used in fault detection (see, e.g., [35]). Furthermore, the system operator could use the results of the online measurement-based contingency selection in (30) and (31) in addition to, or in lieu of, such (potentially erroneous) ac contingency analysis results to formulate the security constraints in the SCED.

3) Security Constraints: We reformulate the line outage security constraints for each line outage mon-con pair, $(\ell_u, c_l^f) \in$

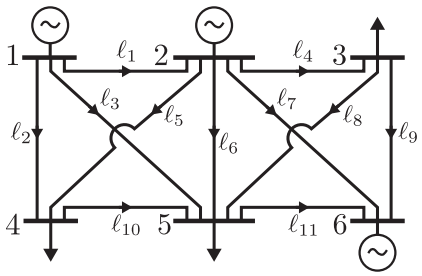

Fig. 1: The 6-bus test system topology.

TABLE I: 6-Bus Generator Offer Function Parameters

generator	a_i (\$/MWh^2)	b_i (\$/MWh)	c_i (\$)
1	0.1100	5.0	150
2	0.0850	1.2	600
6	0.1225	1.0	335

$\mathcal{C}^f$, to reflect the utilization of the measurement-based ISFs as

$$\underline{P}_u^f \leq \hat{\Gamma}_u P + \hat{\Xi}[u,l]\hat{\Gamma}_l P \leq \bar{P}_u^f, \tag{32}$$

where $\hat{\Xi}[u,l]$ is the measurement-based estimate of the LODF of line ℓ_u with respect to the outage of line ℓ_l calculated using the measurement-based ISFs, and those for each generator outage mon-con pair $(\ell_u, c_j^g) \in \mathcal{C}^g$ as

$$\underline{P}_u^f \leq \hat{\Gamma}_u P + (\hat{\Gamma}_u \alpha(c_j^g) e_j^T) P \leq \bar{P}_u^f. \tag{33}$$

With the reformulated network and security constraints in (29) and in (32) and (33), respectively, the real-time SCED no longer relies on a system model. Instead, the system operator continuously updates the estimate of $\hat{\Gamma}$ via (28), and recomputes $\hat{\Xi}$ via (5) and (6), as new PMU measurements become available and uses the most up-to-date estimates to perform contingency selection/analysis, identify and formulate the necessary security constraints, and formulate the real-time SCED. This measurement-based real-time SCED is adaptive to changing system conditions, such as detected or undetected topology changes, variations in bus injections, and even changes in line and other system parameters due to loading or extreme temperature conditions. As such, the dispatch targets and LMPs resulting from the SCED process will reflect real-time system conditions.

A key strength of our proposed measurement-based SCED approach is its consistency with the current real-time SCED framework; the structure of the SCED formulation is left largely unchanged, but more appropriate data is used as the basis for that structure. The result is an enhanced and adaptive real-time SCED. The following case studies demonstrate the adaptability of our measurement-based approach to the real-time SCED.

IV. Case Study I: 6-bus System

We demonstrate the strengths of the proposed measurement-based real-time SCED by using a modified version of the 3-generator, 6-bus test system, shown in Fig. 1, which is provided in the simulation package Matpower [36].

To estimate $\hat{\Gamma}$, we use simulated PMU measurements (assumed to be collected at a measurement frequency of $30/\text{s}$) of the random power injection fluctuations in each load $j \in \mathcal{D}$. These measurements are generated using the nominal load provided with the case according to

$$P_v^d[k] = P_{v,0}^d[k] + \sigma_1 P_{v,0}^d[k]\nu_1 + \sigma_2 \nu_2, \tag{34}$$

where $P_{v,0}^d[k]$ is the case nominal power injection by load v at instant k, and ν_1 and ν_2 are pseudorandom values drawn from a normal distribution with zero mean and standard deviations $\sigma_1, \sigma_2 = 0.01$, respectively ($\sigma_1 P_{j,0}^d[k]\nu_1$ represents random load fluctuations, whereas $\sigma_2\nu_2$ represents measurement noise). We compute simulated PMU measurements of generator power injections $P_i^g[k]$ for each generator $i \in \mathcal{G}$ corresponding to the loads at instant k by solving a distributed slack bus ac power flow with initial generation outputs $P^g[k-1]$, and loads $P^d[k]$, nominal bus reactive power injections Q_0 and voltages V_0 and distributed slack weights, $\gamma \in \mathbb{R}^G$, the entries of which are defined by

$$\gamma_i = \begin{cases} \frac{\bar{P}_i^g}{\sum_{j \in \mathcal{G}_o} \bar{P}_j^g} & \text{if } i \in \mathcal{G}_o, \\ 0 & \text{otherwise,} \end{cases} \tag{35}$$

where $\mathcal{G}_o \subset \mathcal{G}$ is the set of generators with non-zero outputs in the test case nominal power flow solution. In each case studied, we use the simulation package Matpower [36] to compute the relevant line flows. Furthermore, we assume each load has an infinite willingness to pay, i.e., the demand is inelastic, and each generator i, submits a quadratic offer function of the form $a_i(P_i^g)^2 + b_i P_i^g + c_i$, the parameters of which we report in Table I.

A. Selection of M and f

The WLS estimation procedure in (28) has two degrees of freedom: (i) the selection of the number of samples, M, to include in the estimation, i.e. the size of the measurement window; and (ii) the selection of $f \in (0,1]$ so as to specify the diagonal weighting matrix W. A larger measurement window, M, increases the accuracy of the estimation and decreases its susceptibility to noise when the system is in steady state at the expense of increased error when the operation point changes [37]. The selection of f impacts the weight given to the measurements from each measurement instant in the measurement window and choosing $f < 1$ can improve the tracking of the estimator under changing operating conditions at the expense of steady state accuracy [38]. We demonstrate the impacts of the selection of M and f on the ISF estimation with the following series of examples and provide some guidelines for their selection.

To illustrate the impacts on the ISF mean-squared error (MSE) of the selection of M under steady state conditions, we simulate 500 PMU measurements using the process outlined above at the nominal 6-bus power flow solution. Then, we compute the ISFs using (28) with $f = 1$ and with M varied from 20 to 380 measurement instants in increments of 20. The ISF estimates are compared to the 'actual' ISFs, which are computed by repeatedly solving the ac power flow equations around the operating point at each measurement instant with a 0.01 p.u. increase in the net injection at each bus and taking the ratio of line flow changes to the net injection change.

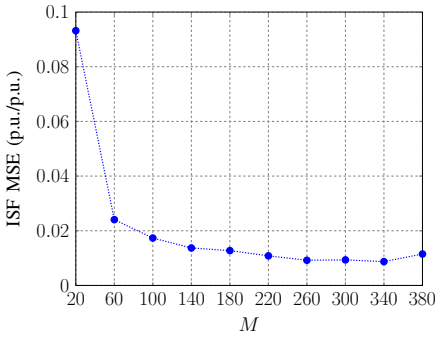

Fig. 2: Sensitivity of the ISF estimation error to the selection of M under steady-state operating conditions with $f = 1$.

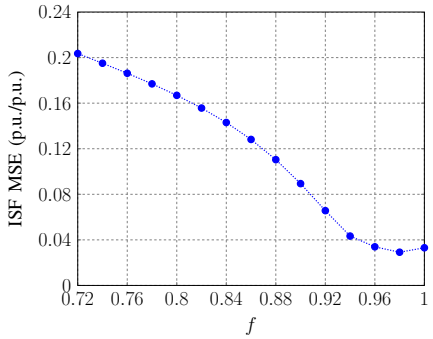

Fig. 3: Sensitivity of the ISF estimation error at instant 350 to the selection of f under changing operating conditions with $M = 120$.

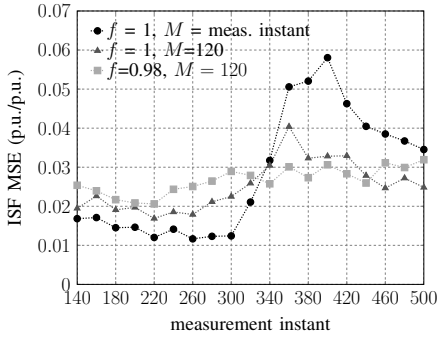

Fig. 4: Impacts on ISF estimation error under changing operating conditions of the selection of M and f.

As shown in Fig. 2, as we increase the value of M, the MSE between the estimated and 'actual' ISFs decreases—substantially between $M = 20$ and $M = 100$ and then slowly for $M > 120$. This finding suggests that one should select as large an M as is computationally feasible. However, when performing the estimation under changing operating conditions, the ISF MSE may not decrease with increasing M, as we show below. Furthermore, the ISF MSE can be improved under changing conditions by selecting $f < 1$.

To demonstrate the impacts on the ISF MSE of the selection of f and M under changing operating conditions, we again simulate 500 PMU measurements, however now we increase the load at bus 4 linearly by 100% between measurement instants 300 and 400, assuming the load increase is balanced by the generators in the system according to the distributed slack policy defined in (35). We then compute four cases of the ISF estimation using (28) with estimation parameters f and M: (i) executed at measurement instance 350 with $M = 120$ and f varied from 0.7 to 1 measurement instants in increments of 0.02; (ii) $f = 1$ and M varied from 140 to 500 measurement instants in increments of 20 and executed at each measurement instance; (iii) with $f = 1$ and $M = 120$ executed at measurement instants 140 to 500 in increments of 20; and (iv) with $f = 0.98$ and $M = 120$ executed at measurement instants 140 to 500 in increments of 20. We select $M = 120$ in these cases based on the the relatively low steady-state ISF MSE found in the above sensitivity study. For each case, we compare the ISF estimates to the 'actual' ISFs computed at the corresponding measurement instant.

As is clear from Fig. 3, the ISF MSE in case (i) is minimized during the operating point change for a fixed M by selecting a value of f close to 1 (or, alternatively, by selecting a value of f such that the weights for oldest measurements in the measurement window do not decay to near zero rendering the measurements ineffectual). As shown in Fig. 4, in case (ii), the MSE increases considerably during the operating point change between measurement instants 300 and 400, due to the inclusion of pre-operating point change data from measurement instants 140 through 300 in the estimation. However, in case (iii), in which we select $f = 1$ and a sliding measurement window of $M = 120$, the MSE is decreased compared to case (ii) during the operating point change as fewer pre-operating point measurements are included in the measurement window throughout the change. Finally, in case (iv), in which we select $f = 0.98$, the ISF MSE when adapting to the operating point change is improved further still due to the bias introduced towards the most recently obtained measurements in the measurement window. However, the ability to track the operating point change in cases (iii) and (iv) comes at the expense of additional steady state MSE, as illustrated by the MSE from measurement instants 140 through 300 for those cases. Thus, there is a tradeoff between the estimator's ability to accurately track changing operating conditions and the steady state accuracy. Our observations from a number of tests carried out on IEEE test systems of varying sizes suggest that for larger-scale systems $M \approx 2N$ and $f \approx e^{\frac{-2.4}{M}}$ are appropriate for balancing tracking and steady-state error.

B. Undetected Line Outage

In this study, we simulate 600 PMU measurements and assume there is an undetected outage of line ℓ_3 at measurement instant 300 and that the real-time SCED is executed at measurement instant 500. We compute the ISFs at each measurement instant beginning with instant 120 using (28) and with $M = 120$ and f = 0.98, and execute the SCED every 20 measurement instants. For buses 1, 2, and 6 (generator buses) and buses 3 through 5 (load buses), and at measurement instants 120 (pre-outage) and 500 (post-outage), Table II shows: (i) the undetected-outage, model-based LMPs, which are the LMPs that would be realized in the presence of

TABLE II: LMPs for Case I-B

bus	model-based LMP ($/MWh)		measurement-based LMP ($/MWh)	
	undetected outage	detected outage	pre-outage	post-outage
1	19.54	17.41	19.54	17.65
2	19.48	13.99	19.48	13.91
3	20.04	30.92	20.04	31.18
4	20.26	20.91	20.25	20.77
5	20.40	52.73	20.40	53.12
6	19.63	30.04	19.63	29.91

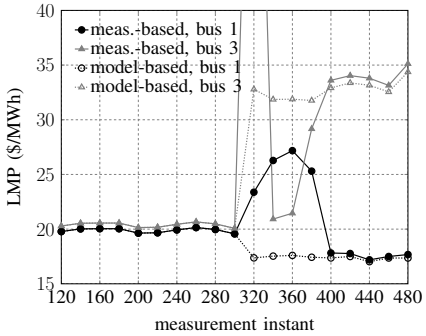

Fig. 5: Measurement- and correct-model-based LMP evolution at a subset of buses with outage of line ℓ_3.

the undetected outage; (ii) the detected-outage, model-based LMPs, which are the LMPs that would be realized if the outage was detected; and (iii) the measurement-based estimates of the LMPs. Unsurprisingly, there is a large discrepancy between the undetected and detected outage model-based LMPs, more than $30/MWh at bus 5. The measurement-based LMPs, however, closely track the correct model-based LMPs regardless of whether or not the outage is detected.

Furthermore, the measurement-based LMPs converge quickly to the correct values following the outage of line ℓ_3. Fig. 5 shows the evolution of the measurement-based and correct-model-based LMPs at buses 1 and 3 (a generator and load bus, respectively) before, during, and after the outage. As shown Fig. 5, the measurement-based LMPs at both buses are nearly coincident with the correct-model-based LMPs prior the the contingency at measurement instant 300, after which there is a period of 100 measurements during which the measurement-based LMPs diverge. However, as the measurement window moves past the pre-outage measurement period, starting at measurement instant 400, the measurement-based LMPs again track the correct-model-based LMP values.

C. Incorrect Data Impacts on Security Analysis

In this study, we simulate 600 PMU measurements and assume the line ℓ_5 impedance data in the model is incorrectly thought to be 20% higher than its true value. The ISFs are again estimated at each measurement instant beginning with instant 120 using (28) and with $M = 120$ and f = 0.98. We run ac contingency analysis with sensitivity-based contingency selection and the real-time SCED at measurement instant 400. Table III shows the overloads identified and SCED LMPs with: (i) the model-based contingency selection and SCED

TABLE III: Identified Overloads and LMPs for Case I-C.

	model-based		
	incorrect data	correct data	measurement-based
identified overload	–	(ℓ_5, c_6^f)	(ℓ_5, c_6^f)
bus	LMP ($/MWh)		
1	19.86	20.99	21.09
2	19.80	19.02	18.96
3	20.36	20.29	20.28
4	20.57	23.62	23.99
5	20.73	21.57	21.66
6	19.95	19.83	19.81

TABLE IV: 118-bus test system modified line limits.

line:	ℓ_8	ℓ_{31}	ℓ_{71}	ℓ_{98}	ℓ_{99}	ℓ_{138}	ℓ_{139}
$\bar{P}^f_{\ell_i}$ (MW):	200	60	50	70	70	70	70

in the presence of the incorrect line data; (ii) the model-based contingency selection and SCED in the presence of the correct line data; and (iii) the measurement-based contingency selection and SCED.

The model-based contingency selection run with the model-based ISFs finds no potential overloads and so no security constraints are added to the model-based SCED formulation. As a result, the model-based SCED with incorrect line data LMPs are similar at all buses, except for differences due to losses. However, with correct line impedance data, contingency selection identifies a potential overload with respect to (ℓ_5, c_6^f), which is confirmed by contingency analysis. As such, a security constraint is added in the model-based SCED formulation with correct line data, which binds on execution producing significantly different LMPs than in the incorrect data case. The measurement-based contingency selection identifies the overload (ℓ_5, c_6^f) and the resulting SCED with the measurement-based security constraints produces LMPs that track those in the model-based case with correct line data.

V. Case Study II: 118-bus System

In this section, we present the results of case studies carried out using a modified IEEE 54-generator, 186-line, 118-bus test system [39], in which a subset of line limits, shown in Table IV, have been reduced so as to introduce transmission congestion. The test system total load is 4242 MW, and total generation capacity is 9966.2 MW and we assume the market operates as a single-clearing-price auction [5]. With these studies, we illustrate the strengths of the proposed measurement-based SCED over the conventional model-based SCED in a larger-scale system.

A. Undetected Line Outage

In this study, we simulate 1500 PMU measurements, which were synthesized using (34), the approach outlined in Section IV, and the nominal 118-bus case power flow solution. Further, we assume there is an undetected outage of the double circuit consisting of lines ℓ_{98} and ℓ_{99} at measurement instant 500 and that the real-time SCED is executed at measurement instant 1400. We compute estimates of the ISFs at each

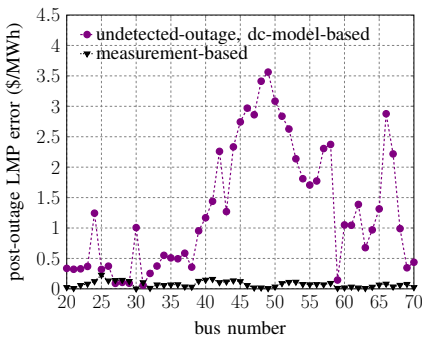

Fig. 6: LMP errors at a highly impacted subset of buses due to the undetected outage of double-circuit ℓ_{98}, ℓ_{99}.

measurement instant beginning with instant 240 using (28) and with $M = 236$ and f = 0.99.

Figure 6 shows the absolute LMP errors for the model-based SCED with an undetected outage and the measurement-based SCED compared to the model-based SCED with the detected outage at a highly impacted subset of buses. The undetected changes in system topology have a significant impact on the prices realized with the real-time SCED process, especially at those buses close to transmission lines at their limit, e.g., buses 49 and 50 or buses 66 and 67. The LMP MSE with the undetected outage in the dc-model-based SCED with respect to the detected-outage, dc-model-based LMPs is \$14.4/MWh across all buses. In contrast, the measurement-based LMPs track the detected-outage, model-based LMPs quite well resulting in an LMP MSE of \$0.90/MWh. This result suggests that the proposed measurement based approach remains accurate as the system size is scaled up.

B. Inaccurate System Model Data

In this study, we simulate the real-time SCED in the presence of erroneous model data. To this end, we perturb the line impedance on each of the top 30% of loaded lines by a random multiple in $[0.7, 1.3]$ drawn from a uniform distribution. We simulate 600 measurements using the same simulated load PMU data used in Case II-A and compute the line flows with the incorrect and correct data. Further, we compute estimates of the ISFs at each measurement instant beginning with instant 240 using (28) and with $M = 236$ and f = 0.99 and assume the real-time SCED is executed at measurement instant 500.

We perform sensitivity-based contingency selection on the 20 and 10 most impactful line and generator contingencies, respectively, to identify overloads. The contingencies that resulted in overloads during contingency analysis (and, in the measurement-based SCED, those that were identified as causing overloads by measurement-based contingency selection) and thus necessitate the formulation of security constraints are reported in Tables V and VI. As reported in Table V, the incorrect model data results in the failure of model-based contingency selection/analysis to identify line contingency pairs (ℓ_{31}, c^f_{70}), (ℓ_{31}, c^f_{74}), (ℓ_{31}, c^f_{82}), and (ℓ_{31}, c^f_{119}). Furthermore, as shown in Table VI, the inaccurate model data results

TABLE V: Identified line outage overloads common to all cases and those unidentified due to incorrect data.

overloaded line #	overload w.r.t. outage of line #
identified overloads common to all cases	
8	33,36,37,51,54
31	16,33,34,36,38,51,54,104,116
71	16,33,34,36,37,38,54,70,74,82,93,94,97,107,116,119
98,99	16,33,34,36,37,38,51,54,74,82,93,94,96,97,104,116,119
138,139	16,33,34,36,37,38,51,54,70,74,82,93,94,96,97,104,107,116,119
overloads unidentified due to bad data	
31	70,74,82,119

TABLE VI: Identified generator outage overloads common to all cases and those mis-identified due to incorrect data.

overloaded line #	overload w.r.t. outage of generator #
identified overloads common to all cases	
8	1,6
31	10,21,22,23,24,25,37,40
71	1,6,10,22,23,24,25,37
98,99	1,6,10,21,22,23,24,25
138,139	1,6,10,21,22,23,24,25,37
overloads mis-identified due to bad data	
71	40

in the incorrect identification of generator contingency pair (ℓ_{70}, c^g_{40}). The unidentified (mis-identified) overloads translate into fewer (additional) constraints in the SCED that subsequently impact the market outcomes. The measurement-based contingency selection, on the other hand, identifies the appropriate contingency overloads and results in the formulation of the correct security constraints.

Figure 7a shows the deviations between the dc-model-based LMPs with correct line impedance data and the bad model data dc-model-based LMPs and measurement-based LMPs. Overall, the measurement-based SCED approach results in LMPs close to those found with the correct line data, the MSE over all buses is \$1.67/MWh compared to \$5.25/MWh for the incorrect data dc-model. However, there are some deviations between the model-based with correct data and measurement-based approaches. To give some insight into the nature of these differences, Fig. 7b shows the correct-data, dc-model-based LMPs and measurement-based LMPs compared to LMPs computed by running the SCED with 'actual' ISFs calculated by repeatedly solving the ac power flow.

When compared to the 'actual' model-based LMPs, the measurement-based LMPs perform much better than the dc-model-based LMPs, the MSE is \$0.23/MWh compared to the \$1.78/MWh for the correct-data, dc-model-based LMPs. This finding suggests that the measurement-based SCED approach is able to capture information that the dc-model-based SCED approach does not, e.g., the impacts of reactive power and voltage changes in response to active power injection changes on active power flows, which is subsequently reflected in the LMPs. As such, the differences between the measurement-base LMPs and correct-data, dc-model-based LMPs, reported in Fig. 7a, may actually be indicative of errors in the correct-data, dc-model-based LMPs related to the underlying dc assumptions; the measurement-based approach requires the assumption that the relationship between active power injections

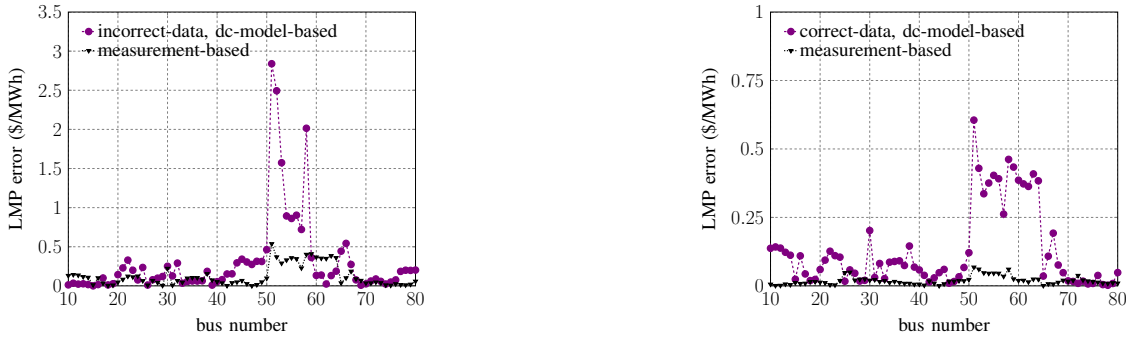

(a) LMP errors w.r.t. dc-model with correct data LMPs.

(b) LMP errors w.r.t. linearized ac-model with correct data LMPs.

Fig. 7: Model-based and measurement-based absolute LMP errors due to the incorrect model data for heavily loaded lines with respect to correct data, dc-model and 'actual' LMPs at a highly impacted subset of buses.

and active power flows is linear, however it does not require the dc assumptions and thus is not impacted by the error introduced by those assumptions.

C. Computational Speed and ISF Accuracy

In the real-time power system operations environment, time is a scare commodity and thus fast computation is a necessity. Indeed, most ISOs/RTOs execute state estimation and contingency analysis on a one-minute basis (see, e.g., [31]) and the SCED on a five-minute basis (see, e.g., [2]). As such, the proposed measurement-based SCED must attain reasonable accuracy with no more computation than conventional processes, in order for it to be useful in this context.

Table VII reports for each of the SCED case studies: (i) the computation time for executing one ISF estimation prior to the SCED, the MSE between the measurement-based ISFs and the 'actual' ISFs (computed, as before, by repeatedly solving the ac power flow); and (ii) the computation time for computing the model-based ISFs and the MSE between the bad data/undetected outage model-based ISFs and 'actual' ISFs. Additionally, the SCED computation time is reported for each case; the computation times for the SCED were found to be nearly identical with the model- and measurement-based approaches, so we don't differentiate between them in the table. For reference, all case studies were carried out using Matlab on a MacBook Pro with a 3 GHz Intel Core i7 processor and 16 GB of memory.

In all cases, the measurement-based ISF MSE is an order of magnitude less than that for the model-based ISFs, which provides additional explanation for the observed differences in the LMPs reported above. Additionally, the time required to compute an estimate of the ISFs is on the order of the time required to compute them via the model-based approach. However, we note that the ISF computation times reported for the model-based approach do not include the additional time that would be required in practice to execute topology processing and state estimation. Thus, we are confident that with a state-of-the-art implementation, the measurement-based SCED could be executed within the time constraints of real-time operations.

TABLE VII: Comparison of case study computation times and ISF accuracy.

	meas.-based		model-based		
Case	ISF est. comp. time (ms)	ISF MSE (p.u./p.u.)	ISF comp. time (ms)	ISF MSE (p.u./p.u.)	SCED comp. time (ms)
I-B	0.011	0.059	0.367	1.26	5.4
I-C	0.011	0.046	0.367	1.28	16
II-A	4.01	0.479	2.54	16.3	33
II-B	4.02	0.250	2.54	16.4	51

VI. Concluding Remarks

In this paper, we proposed a measurement-based approach to the real-time SCED. Our approach leverages sensitivities estimated from PMU measurements to perform contingency selection and formulate security constraints, as well as to reformulate the model-based power flow and network flow constraints of the existing model-based real-time SCED. As shown in our case studies, the measurement-based real-time SCED is robust to undetected system disturbances and inaccurate model data and results in market outcomes that more accurately reflect real-time system conditions.

Our future work will focus on the evaluation of the comparative performance of the measurement-based vs model-based real-time SCED in interconnected systems with little or no information exchange. Moreover, we will explore measurement-based methods to compute the loss factors.

Appendix

Nomenclature

Indices:

i, j	indices of generators
v	index of loads
l, u	indices of lines
n, m	indices of buses
k	index of discrete time intervals
t	index of continuous time
$\ell_l = (n, m)$	ordered pair denoting line l is from n to m
(ℓ_u, c_j^g)	ordered pair denoting overload of line ℓ_u due to contingency of generator j
(ℓ_u, c_l^f)	order pair denoting overload of line ℓ_u due to contingency of line ℓ_l

Sets:

$\mathcal{N}$	set of N buses
$\mathcal{L}$	set of L lines
$\mathcal{G}$	set of G generators
$\mathcal{G}_n$	set of generators at bus n
$\mathcal{D}$	set of D loads
$\mathcal{D}_n$	set of loads at bus n
$\mathcal{C}^f$	set of line outage mon-con pairs
$\mathcal{C}^g$	set of generator outage mon-con pairs

Scalars:

P_n	net injection at bus n
P_i^g	output of generator i
P_v^d	demand of load v
P_l^f	flow on line ℓ_l
P^ℓ	system-wide losses
$\Delta P_n(t)$	change in injection at bus n at time t
$\Delta P_{l,n}^f(t)$	change in flow on line ℓ_l due to change in injection at bus n at time t
M	number of synchronized measurements
f	exponential weight parameter
λ^r	dual variable of power balance constraint
ν_1 (ν_2)	zero mean normal random variable with standard deviation σ_1 (σ_2)

Vectors:

P	net injections at all buses $n \in \mathcal{N}$
P^g	outputs of all generators $i \in \mathcal{G}$
P^d	demands of all loads $v \in \mathcal{D}$
P^f	flow on all lines $\ell_l \in \mathcal{L}$
$\underline{P}^g$ ($\bar{P}^g$)	generator output lower (upper) limits
$\underline{P}^d$ ($\bar{P}^d$)	load demand lower (upper) limits
$\underline{P}^f$ ($\bar{P}^f$)	line flow lower (upper) limits
$\underline{P}^s$ ($\bar{P}^s$)	security constraint lower (upper) limits
$\underline{\mu}$ ($\bar{\mu}$)	flow constraint lower (upper) limit dual variables
$\underline{\mu}^s$ ($\bar{\mu}^s$)	security constraint lower (upper) limit dual variables
ζ	bus marginal loss sensitivity vector
$\mathbb{1}_N$	N-dimensional all-ones vector
Ψ_l	lth row of ISF matrix
Γ_l	lth row of measurement-based ISF matrix
$\alpha(c_j^g)$	nodal outage participation factors for outage of generator j
e_j	N-dimensional vector with 1 in entry j and zero elsewhere
ΔP_l^f	collection of M flow change measurements on line ℓ_l

Matrices:

Ψ	ISF matrix
Φ_l	PTDF matrix for line ℓ_l
Ξ	LODF matrix
Ψ^s	security constraint sensitivity matrix
Γ	measurement-based ISF matrix
W	diagonal weighting matrix
ΔP	collection of M net injection change measurements for each of the N buses

Functions:

$\mathscr{S}(P^g, P^d)$	social surplus
$\mathscr{B}_v(P_v^d)$	bid function of load v
$\mathscr{C}_i(P_i^g)$	offer function of generator i

REFERENCES

[1] "2009 state of the markets report," ISO/RTO Council, Tech. Rep., 2010.

[2] California Indendent System Operator. (2014, accessed Nov. 4, 2014) CAISO markets and processes. [Online]. Available: http://www.caiso.com/Documents/Section27CAISOMarketsAndProcessesOct12014.pdf

[3] Independent System Operator of New England. (2014, accessed Nov. 4, 2014) M-11 market operations. [Online]. Available: http://www.iso-ne.com/participate/rules-procedures/manuals

[4] A. Ott, "Experience with PJM market operations, system design, and implementation," *IEEE Trans. Power Syst.*, vol. 18, no. 2, pp. 528–534, May 2003.

[5] B. Wood, B. Wollenberg, and G. Sheblé, *Power Generation, Operation, and Control*, 3rd ed. John Wiley and Sons, Inc., 2014.

[6] NERC. (2007, Accessed: Dec. 9, 2014) Reliability concepts v 1.0.2. [Online]. Available: http://www.nerc.com/files/concepts_v1.0.2.pdf

[7] O. Alsaç and B. Stott, "Optimal load flow with steady-state security," *IEEE Trans. Power App. Syst.*, vol. PAS-93, no. 3, pp. 745–751, May 1974.

[8] F. Capitanescu, J. Martinez Ramos, P. Panciatici, D. Kirschen, A. Marano Marcolini, L. Platbrood, and L. Wehenkel, "State-of-the-art, challenges, and future trends in security constrained optimal power flow," *Electric Power Systems Research*, vol. 81, no. 8, pp. 1731 – 1741, 2011.

[9] A. Ardakani and F. Bouffard, "Identification of umbrella contraints in dc-based security-constrained optimal power flow," *IEEE Trans. Power Syst.*, vol. 28, no. 4, pp. 3924–3934, Nov. 2013.

[10] Y. Liu, M. Ferris, and F. Zhao, "Computational study of security constrained economic dispatch with multi-stage rescheduling," *IEEE Trans. Power Syst.*, vol. 30, no. 2, pp. 920–929, Mar. 2015.

[11] Y. Chen and P. Gribik, "Incorporating post zonal reserve deployment transmission constraints into energy and ancillary service co-optimization," *IEEE Trans. Power Syst.*, vol. 29, no. 2, pp. 537–549, Mar. 2014.

[12] F. Bouffard, F. Galiana, and A. Conejo, "Market-clearing with stochastic security—part I: Formulation," *IEEE Trans. Power Syst.*, vol. 20, no. 4, pp. 1818–1826, Nov. 2005.

[13] A. Sakis Meliopoulos, B. Fardanesh, and S. Zelingher, "Power system state estimation: Modeling error effects and impacts on system operation," in *Proc. of Hawaii International Conference on System Sciences*, Jan. 2001.

[14] K. Poon, R. Emami, A. Bose, and A. Abur, "External data exchange issues for state estimation in power systems," *IEEE Trans. Power Syst.*, vol. 27, no. 2, pp. 849–856, May 2012.

[15] IEEE Working Group D6, "AC transmission line model parameter validation," Prepared for the Line Protection Subcommittee of the Power System Relay Committee of the IEEE Power & Energy Society, Tech. Rep., 2014.

[16] M. Bŏkarjova and G. Andersson, "Transmission line conductor temperature impact on state estimation accuracy," in *Proc. of IEEE POWERTECH Conference*, July 2007.

[17] NERC, "Lesson learned: Real-time contingency analysis failure due to a modeling error," June 2015.

[18] U.S.-Canada Power System Outage Task Force. (2004, accessed Feb 12, 2015) Final report on the August 14, 2003 blackout in the United States and Canada: Causes and recommendations.

[19] NERC and FERC. (2012, accessed Nov. 4, 2014) Arizona-southern california outages on september 8, 2011.

[20] Y. Chen, A. Domínguez-García, and P. Sauer, "Measurement-based estimation of linear sensitivity distribution factors and applications," *IEEE Trans. Power Syst.*, vol. 29, no. 3, pp. 1372–1382, May 2014.

[21] ——, "A sparse representation approach to online estimation of power system distribution factors," *IEEE Trans. Power Syst.*, to appear.

[22] E. Makram, M. Vutsinas, A. Girgis, and Z. Zhao, "Contingency analysis using synchrophasor measurements," *Electric Power Systems Research*, vol. 88, pp. 64–68, 2012.

[23] Y. Chen, A. Domínguez-García, and P. Sauer, "Generalized injection shift factors and application to estimation of power flow transients," in *Proc. of North American Power Symposium*, Pullman, Wa, 2014.

[24] A. Monticelli, *State Estimation in Electric Power Systems: A Generalized Approach*. Kluwer Academic Publishers, 1999.

[25] California Indendent System Operator. (2014, accessed Jan. 4, 2015) Business practice manual for manging full network model. [Online]. Available: http://bpmcm.caiso.com/Pages/BPMDetails.aspx?BPM=Managing%20Full%20Network%20Model

[26] K. Van Horn, A. Domínguez-García, and P. Sauer, "Measurement-based real-time economic dispatch," in *Proc. of IEEE Power and Energy Society General Meeting*, 2015 [Preprint available upon request].

[27] D. Kirschen and G. Strbac, *Fundamentals of Power System Economics*. West Sussex, England: John Wiley and Sons Ltd., 2004.

[28] B. Stott, J. Jardim, and O. Alsaç, "DC power flow revisited," *IEEE Trans. Power Syst.*, vol. 24, no. 3, pp. 1290–1300, Aug. 2009.

[29] D. Kothari and J. Dhillon, *Power System Optimization*, 1st ed. PHI Leanring Private Limited, 2011.

[30] A. Monticelli, M. Pereira, and S. Granville, "Security-constrained optimal power flow with post-contingency corrective rescheduling," *IEEE Trans. Power App. Syst.*, vol. 2, no. 1, pp. 175–180, Feb. 1987.

[31] J. Dondeti, P. Addepalle, C. Yang, and B. Buescher, "MISO experiences of network model maintenance — state estimator and contingency analysis accuracy," in *IEEE Power and Energy Society General Meeting*, July 2014.

[32] X. Cheng and T. Overbye, "An energy reference bus independent LMP decomposition algorithm," *IEEE Trans. Power Syst.*, vol. 21, no. 3, pp. 1041–1049, Aug. 2006.

[33] T. Orfanogianni and G. Gross, "A general formulation for LMP evaluation," *IEEE Trans. Power Syst.*, vol. 22, no. 3, pp. 1163–1173, Aug. 2007.

[34] Electric Power Group. (2014, accessed June 1, 2015) Synchro-phasor data conditioning and validation project phase 1, task 3 report: Algorithms and methods for data validation and conditioning. [Online]. Available: https://www.naspi.org/File.aspx?fileID=1306

[35] R. Isermann, *Fault-Diagnosis Systems: An introduction from fault detection to fault tolerance*. Springer, 2006.

[36] R. Zimmerman, C. Murillo-Sanchez, and R. Thomas, "Matpower: Steady-state operations, planning and analysis tools for power systems research and education," *IEEE Trans. Power Syst.*, vol. 26, no. 1, pp. 12–19, Feb. 2011.

[37] S. Haykin, *Adaptive filter theory*. Prentice Hall, 1996.

[38] L. Ljung and T. Söderström, *Theory and practice of recursive identification*. MIT Press, 1983.

[39] University of Washington. (1993, accessed Nov. 20, 2014) Power systems test case archive. [Online]. Available: http://www.ee.washington.edu/research/pstca/pf118/pg_tca118bus.htm